ELSEVIER

Applied Surface Science 116 (1997) 293–299

applied surface science

Two-component density-functional calculations for positrons trapped by defects in solids

M.J. Puska [a,*], T. Korhonen [a], R.M. Nieminen [a], A.P. Seitsonen [a,b]

[a] *Laboratory of Physics, Helsinki University of Technology, Fin-02150 Espoo, Finland*
[b] *Fritz-Haber-Institut der Max-Planck-Gesellschaft, Faradayweg 4–6, D-14195 Berlin–Dahlem, Germany*

Received 2 June 1996; accepted 2 June 1996

Abstract

We present results of two-component density-functional calculations for electron systems with a localized positron. The theory is implemented into several electronic-structure calculation methods. For example, positron states at vacancies in semiconductors have been calculated in the pseudopotential plane-wave framework. The ionic relaxations, including the positron induced relaxation, have been determined in this scheme by first-principles molecular-dynamics methods. Positron states localized at vacancies in metals have been calculated using the tight-binding linear muffin–tin-orbital method within the atomic-spheres approximation as well as using the full-potential linear muffin–tin-orbital method. Calculations have been performed for positron lifetimes, core annihilation lineshapes and two-dimensional angular correlation maps. The results are compared with experiment.

PACS: 71.10.− w; 71.60.+ z; 78.70.Bj

Keywords: Positron states; Computational techniques; Positron annihilation; Density functional theory

1. Introduction

A positron interacting with electrons of a solid constitutes a many-body problem in which one has to go beyond the independent particle approximation (IPM) in order to describe positron annihilation characteristics. Using the two-component density-functional theory (TCDFT) [1] this can be done in practice. The theory introduces (average) electron and positron densities, by the help of which the total energy of the system can be expressed. Moreover, it leads to the generalized Kohn–Sham equations for calculating these densities. Finally, it shows how the positron annihilation characteristics can be calculated.

There has been thus far, however, only a few calculations employing the TCDFT so that the electron and positron densities are calculated self-consistently and simultaneously [1–4]. This is because this kind of self-consistent calculations are computationally demanding, and because the knowledge about the electron–positron correlation functionals needed in the theory has been quite scarce. Moreover, when calculating positron states delocalized in perfect periodic lattices, the positron does not influence the average electron density, and self-consistency itera-

* Corresponding author. Tel.: +358-9-451-3101; fax: +358-9-451-3116; e-mail: martti.puska@hut.fi.

PII S0169-4332(96)01072-0

tions with respect to the positron density are not needed. Only a localized positron affects, due to the finite positron density, the average electron density. It may also affect the positions of the ions around the defect.

In this paper we will review the results of TCDFT calculations [3,5] for positrons trapped by vacancies in metals and in semiconductors. The results are compared with those obtained with the so-called conventional method (CONV). In the CONV method the localized positron does not affect the average electron density and its potential and annihilation characteristics are calculated as for a delocalized positron. In order to attain conclusive results about the properties of different schemes, the annihilation characteristics calculated should be numerically stable against approximations *within* a given computational method. Moreover, a convergence *between* different numerical methods should be reached. It turns out that the calculation of the localized positron state has to be done very carefully. For instance, the relatively large extent of the positron wave function makes its proper normalization and the finding of the correct positron density at the defect to non-trivial tasks.

2. Two-component density-functional theory

In the TCDFT the (average) electron ($n_e(\boldsymbol{r})$) and positron ($n_p(\boldsymbol{r})$) densities are calculated from single-particle wave functions obtained from the Kohn–Sham single-particle Schrödinger equations. One has to sum up electron states up to the Fermi level but there is only one positron in the system. The effective potential for the electrons reads as

$$V_e^{\mathrm{eff}}(\boldsymbol{r}) = -\phi\left[\{Z_I, \boldsymbol{R}_I\}, n_e, n_p\right] + v_{xc}(n_e(\boldsymbol{r})) + \frac{\delta}{\delta n^e} E_{\mathrm{corr}}[n_e, n_p], \quad (1)$$

where $\phi[\{Z_I, \boldsymbol{R}_I\}, n_e, n_p]$ is the Coulomb potential due to nuclei (charges Z_I and positions $\boldsymbol{R}_I$) and due to the electron and positron densities. v_{xc} is the exchange-correlation potential for the electron subsystem. We use the local density approximation (LDA) for v_{xc}. $E_{\mathrm{corr}}[n_e, n_p]$ is the electron–positron correlation energy and the functional derivative with respect to the electron density gives a contribution to the electron potential. Based on Lantto's hypernetted-chain calculations [6] we have introduced for $E_{\mathrm{corr}}[n_e, n_p]$ a new (two-dimensional) interpolation formula [3] within the LDA.

The effective positron potential is written as

$$V_e^{\mathrm{eff}}(\boldsymbol{r}) = +\phi\left[\{Z_I, \boldsymbol{R}_I\}, n_e\right] + \frac{\delta}{\delta n^p} E_{\mathrm{corr}}[n_e, n_p], \quad (2)$$

Compared to the electron potential the sign of the Coulomb part is reversed and the correlation potential is obtained as a functional derivative with respect to the positron density. Note also that, in comparison with Eq. (1), a self-interaction correction has been made: The Coulomb potential does not depend on the positron density and there is no exchange-correlation potential depending on the positron density.

In the TCDFT calculations within the LDA the positron annihilation rate as a function of the momentum $\boldsymbol{p}$ of the annihilating positron–electron pair is obtained as

$$\rho(\boldsymbol{p}) = \pi r_e^2 c \sum_i \times \left| \int e^{i\boldsymbol{p}\cdot\boldsymbol{r}} \psi_p(\boldsymbol{r}) \psi_e(\boldsymbol{r}) \sqrt{g\left(n_e(\boldsymbol{r}), n_p(\boldsymbol{r})\right)}\, d\boldsymbol{r} \right|^2, \quad (3)$$

where r_e is the classical electron radius and c is the speed of light. The summation is over all occupied electron states. The enhancement factor $g(n^e, n^p)$ takes into account the difference between the 'real' contact density and the product of average densities. We use for $g(n^e, n^p)$ the interpolation form [3] based on Lantto's data [1]. The enhancement factor decreases with increasing electron or positron density. The positron lifetime τ is calculated as the inverse of the total annihilation rate λ which is obtained from Eq. (3) by integrating over the momentum,

$$\lambda = \pi r_e^2 c \int d\boldsymbol{r}\, n_p(\boldsymbol{r})\, n_e(\boldsymbol{r})\, g\left(n_e(\boldsymbol{r}), n_p(\boldsymbol{r})\right). \quad (4)$$

3. Delocalized positron states and the conventional scheme

In the case of a delocalized positron in a perfect lattice, the positron density is everywhere vanish-

ingly small. Then the positron density does not affect the average bulk electronic structure. The electron potential is obtained from Eq. (1) by canceling the positron density in the Coulomb potential and the contribution due to the electron–positron correlation. In the positron potential (Eq. (2)) the electron–positron correlation part depends only on the electron density. These simplifications mean that the electronic structure is first calculated self-consistently without the effect of the positron. Then the positron state is determined without any self-consistency iterations. The annihilation characteristics are obtained from Eqs. (3) and (4) by using the enhancement factor on the limit of the vanishing positron density, i.e. the enhancement factor does not depend on the positron density.

The simplicity of the calculations of delocalized positron states is adopted in the CONV scheme also to the calculation of localized positron states at defects in solids. This means that the formalism for a delocalized positron state is used in spite of the finite positron density. The scheme can be justified by thinking that the positron with its electron screening cloud form a neutral quasiparticle which can enter the system without affecting the average electron density.

4. Numerical methods

We have used in the calculation of positron states and annihilation characteristics several numerical methods. For the defects in semiconductors we have used a method [3] in which the valence electron density is constructed within the pseudo-potential plane-wave framework and the positron wave function is solved on a real-space mesh [7]. The real-space techniques enables an easy and accurate construction of the positron potential from the valence electron density and from the core charge distribution of a free atom. The Hellman–Feynman forces (including the influence of the localized positron) acting on ions are calculated and the ensuing ionic relaxations are solved. TCDFT as well as CONV scheme calculations have been performed.

For defects in metals we have used all-electron methods. In the tight-binding version [8] of the linear muffin–tin-orbital method within the atomic-spheres approximation (LMTO-ASA) (for a recent review, see [9]) the crystal volume is divided into overlapping atom-centered spheres and the potential and the charge densities are assumed to be spherically symmetric inside each sphere. A vacancy defect, for instance, means in the LMTO-ASA an 'empty' vacancy sphere in the crystal. The electron and positron wave functions are constructed by using partial spherical waves. We have used for defects in metals also the full-potential linear muffin–tin-orbital (FP-LMTO) method [10]. Also this method employs partial waves for the construction of wave functions but it makes no shape approximation to the potentials or to the charge densities. With the FP-LMTO method we have performed only CONV scheme calculations whereas the LMTO-ASA method has been used also for TCDFT calculations.

Parallel to the above described calculations with electronic structures self-consistent within the CONV or TCDFT schemes we have also employed the atomic superposition (ATSUP) method [11]. In this method the electronic structure is obtained simply by overlapping free-atom charge densities. The method does not imply any further geometrical shape approximations. For a system with given ionic positions, the electron density and the positron potential are constructed on the points of a real-space mesh using the CONV scheme. The resulting three-dimensional Schrödinger equation for the positron state is solved in a real-space point mesh [7] which is used also to calculate the positron annihilation rate. The ATSUP method is very effective compared to the methods using self-consistent electron densities.

In all the above numerical methods we have used the supercell approximation to describe the defect in question. This means that, for instance, an isolated vacancy is replaced by a periodic vacancy structure, and the electronic as well as the positron structure is solved using periodic boundary conditions for the wave functions. For too small supercell sizes there are interactions between the vacancies of the superlattice and the approximation does not describe well an isolated vacancy. The effects have been discussed in the context of the electronic-structure calculations for defect total energies [12,13]. It has been shown that by a careful sampling of the superlattice Brillouin-zone one can reduce the effects of the defect-defect interactions. We have shown that this is true

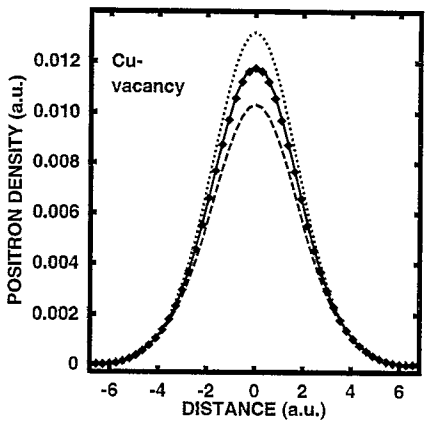

Fig. 1. Positron density at the Cu vacancy. The density is given along a line in the [100] direction and passing through the center of the vacancy. The ATSUP method has been used. The solid line corresponds to a Γ-point calculation with a supercell size of $N = 256$ lattice sites, the dashed line to a Γ-point and the dotted line to a k-point on the BZ-surface with a supercell size of $N = 32$. The markers are the average of results corresponding the two k-points and $N = 32$.

also for the positron states, and for the ensuing annihilation characteristics [5]. Briefly, for the Γ-point the positron wave function has the same sign in the whole superlattice and a finite value on the cell boundaries. When using other k-points the positron density at the cell boundaries is reduced. In the case of a simple cubic supercell the positron wave function at the cell boundaries vanishes for the L-point (on the zone boundary in a $\langle 111 \rangle$ direction). In order to find the positron density close to that for an isolated vacancy one has to take the proper average from the densities for different k-points. Fig. 1 shows that for a Cu vacancy treated by a simple cubic superlattice the sampling using the Γ and L-points gives with a small supercell size a density which is very close to that for a much larger supercell, i.e. for that representing an isolated vacancy. The sampling leads then to a fast convergence of the positron lifetime as show in Fig. 2. We have found that also other k-point samplings may be quite effective. For example, according to our experience the use of the k-point between the Γ and L-points gives quite well converged results for positron states at vacancies in metals and in semiconductors.

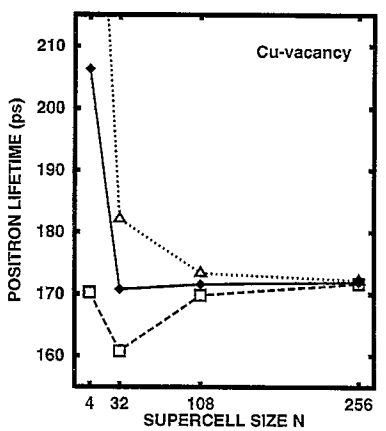

Fig. 2. Calculated positron lifetimes for the Cu vacancy as a function of the supercell size N. The ATSUP method has been used. The dashed line corresponds to the Γ-point calculations, the dotted line to a k-point on the BZ-surface calculations, and the solid line to the BZ-integration calculations, i.e. the average of the Γ-point and a k-point on the BZ-surface densities is used.

5. Results

Fig. 3 compares the positron and electron densities obtained in the CONV and TCDFT schemes [5]. The distributions are calculated for a positron trapped by a vacancy in Cu using the LMTO-ASA method. The difference between electron densities of the TCDFT and the CONV schemes gives how much the localized positron can raise the average electron density in the TCDFT description. The positron dis-

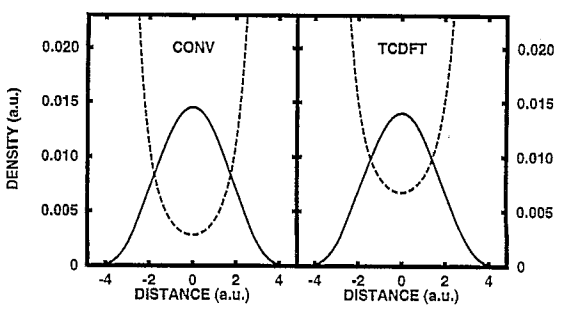

Fig. 3. Positron (————) and electron (– – –) densities at the Cu vacancy. The densities are given along a line in the [110] direction and passing through the center of the Cu vacancy. Shown are the results of the TCDFT and CONV scheme calculations by the LMTO-ASA method.

tributions are very similar between the two schemes. This is because, relative to the CONV scheme, the correlation potential in the TCDFT scheme decreases when the positron density increases and this opposes the lowering of the Hartree part due to the increase in the electron density at the defect. Therefore the effective positron potentials are similar resulting in quite identical positron densities.

Positron lifetimes calculated [5] for vacancies in several fcc and bcc metals are shown in Fig. 4. The positron bulk lifetimes are given for comparison. The results obtained in the TCDFT and CONV schemes using the LMTO-ASA method are very similar. Relative to the CONV scheme the larger electron–positron overlap in the TCDFT scheme tries to increase the annihilation rate but this increase is opposed by the decrease of the enhancement factor as the positron density increases. The different computational methods give in the CONV scheme positron lifetimes within a few picoseconds from each other. The LMTO-ASA and the FP-LMTO results are on the average closer to each other than to the ATSUP results. This shows the role of the self-consistent electronic structure. All the theoretical estimates for the positron lifetimes are in a fair agreement with the experimental results. The ratios τ_v/τ_b between the vacancy and the corresponding bulk lifetimes are given in Fig. 5. The ratios are useful for comparing theoretical and experimental results. This is because these ratios are not very sensitive to the models for the positron–electron correlation or for the enhancement used [14]. Also systematic experimental errors

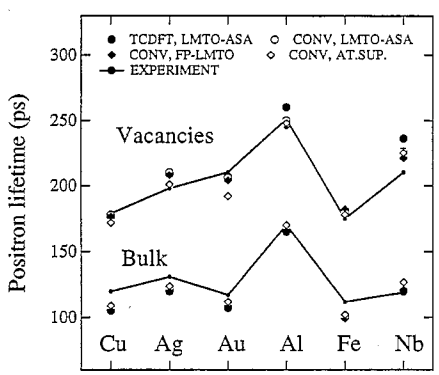

Fig. 4. Calculated and experimental positron lifetimes for metal vacancies. The experimental lifetimes for Cu, Ag, Au, Al, Fe and Nb are from Refs. [20], [21], [22], [23], [24] and [25], respectively.

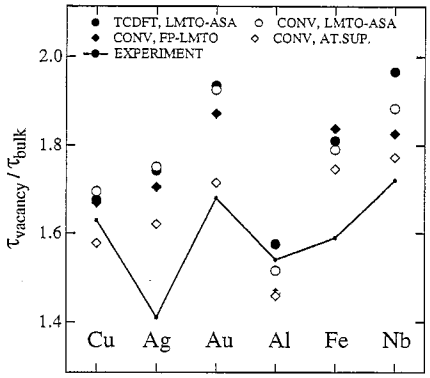

Fig. 5. Ratios of the positron lifetimes between metal vacancies and perfect bulk lattices. For the experimental references, see the caption of Fig. 4.

are expected partly to cancel in the ratios. According to Fig. 5 the methods using self-consistent electron densities give systematically larger ratios than the ATSUP method or the measurements. The difference between the experiment and the calculations employing self-consistent electron densities suggest that the ions neighboring the vacancy should relax inwards. As a matter of fact, this is the result of first-principles electronic-structure calculations [13,15].

We have performed TCDFT calculations for the positron state trapped by the Ga vacancy in the III–V semiconductor GaAs [3]. The vacancy is in the triply-negative charge state, which corresponds to the situation in semi-insulating or n-doped samples. The calculation is done by using the pseudo-potential plane-wave scheme for the valence electron states whereas the positron wave function is obtained on a real-space mesh using free-atom core densities in describing the positron–ion interactions. The ions are allowed to relax as a response to the Hellmann–Feynman forces due to the electronic structure as well as the localized positron state. Without the positron the ions neighboring the Ga vacancy relax symmetrically inwards about 11% of the ideal lattice bond length. The trapped positron pushes the nearest ions outwards so that the inward relaxation is about 7% of the bond length. This calculation is made by using a 63 atom supercell and only the Γ-point in the Brillouin-zone sampling. Therefore the positron wave function may be slightly too delocalized and its effects to the ionic relaxation underestimated. This is

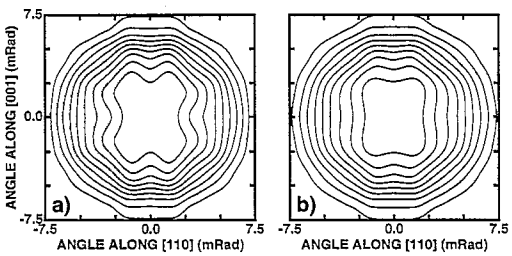

Fig. 6. Angular correlations of annihilation photons corresponding to the (a) bulk GaAs and (b) the triply-negative Ga vacancy in GaAs. The momentum distributions are integrated along the [110] direction. The results are based on the self-consistent solution for the electronic structure, positron state and the ionic positions at the vacancy within TCDFT scheme [3]. The contour spacing is one tenth of the maximum value.

reflected in the ratio between the positron lifetimes for the vacancy and for the perfect bulk. According to our TCDFT calculation the ratio is 1.04, which is clearly smaller than the experimental ratio of 1.12 [16]. However, already rather small changes in the ionic relaxation can bring the theory and experiment into agreement [3].

We have calculated the maps of the two-dimensional angular correlation of annihilation radiation (2D-ACAR) for the positron delocalized in bulk GaAs and trapped by a triply-negative Ga vacancy in GaAs [3]. The results are shown in Fig. 6. The trapping increases the isotropy of the distribution. According to experiments [16] the isotropy is somewhat larger which again calls for a better positron localization at the vacancy.

The relative core annihilation parameter W describes the changes in the percentage of core annihilation contribution between a positron trapped by a defect and a free positron [17]. It can be calculated from the momentum distributions of the annihilating electron–positron pairs [18]. However, a rather good estimate may be obtained from the total annihilation rates with the core and valence electrons [18]. Our TCDFT calculations [3] for the triply-negative Ga vacancy in GaAs give a W parameter estimate of 0.88. This is somewhat larger than the experimental value of 0.74 [18] indicating again that the positron localization at the vacancy is too weak. For the vacancy in Al we predict a W parameter of the order of 0.3. This is clearly smaller than those for vacancies in semiconductors. In all cases the TCDFT and the CONV schemes give quite similar positron lifetimes, momentum distributions of annihilating electron–positron pairs as well as W parameters.

6. Conclusions

First-principles calculations of annihilation characteristics for positrons trapped by defects in solids have reached the level of a high quantitative predictive power. This is true especially for relative measures such as the ratios of the quantities for defects and perfect bulk lattices. The prediction of the absolute values may still be a subtle question [18,19]. In the calculations the self-consistent determination of the ionic relaxation is an important ingredient especially for defects in semiconductors. The full two-component calculation of the electron and positron densities may be largely avoided and the positron characteristics calculated within the conventional scheme. The computational methods show convergence with respect to the internal approximations such as the supercell size and the results of different methods are in good agreement.

References

[1] E. Boroński and R.M. Nieminen, Phys. Rev. B 34 (1986) 3820.
[2] L. Gilgien, G. Galli, C. Gygi and R. Car, Phys. Rev. Lett. 72 (1994) 3214.
[3] M.J. Puska, A.P. Seitsonen and R.M. Nieminen, Phys. Rev. B 52 (1995) 10947.
[4] M. Saito and A. Oshiyama, Phys. Rev. B 53 (1996) 7810.
[5] T. Korhonen, M.J. Puska and R.M. Nieminen, Phys. Rev. B, submitted.
[6] L. Lantto, Phys. Rev. B 36 (1987) 5160.
[7] A.P. Seitsonen, M.J. Puska and R.M. Nieminen, Phys. Rev. B 51 (1995) 14057.
[8] O.K. Andersen, O. Jepsen and D. Glötzel, in: Highlight of Condensed-Matter Theory, Eds. F. Bassani, F. Fumi and M.P. Tosi (North-Holland, New York, 1985).
[9] O.K. Andersen, O. Jepsen and M. Šob, in: Electronic Band Structure and its Applications, Ed. M. Yussouff (Springer-Verlag, Heidelberg, 1987).
[10] M. Methfessel, Phys. Rev. B 38 (1988) 1537; M. Methfessel, C.O. Rodriguez and O.K. Andersen, Phys. Rev. B 40 (1989) 2009.
[11] M.J. Puska and R.M. Nieminen, J. Phys. F 13 (1983) 333.
[12] J. Furthmüller and M. Fähnle, Phys. Rev. B 46 (1992) 3839.

[13] N. Chetty, M. Weinert, T.S. Rahman and J.W. Davenport, Phys. Rev. B 52 (1995) 6313.
[14] B. Barbiellini, M.J. Puska, T. Korhonen, A. Harju, T. Torsti and R.M. Nieminen, Phys. Rev. B, in print.
[15] M.J. Mehl and B.M. Klein, Physica B 172 (1992) 211; R. Benedek, L.H. Yang, C. Woodward and B.I. Min, Phys. Rev. B 45 (1992) 2607.
[16] P. Hautojärvi, P. Moser, M. Stucky, C. Corbel and F. Plazaola, Appl. Phys. Lett. 48 (1986) 809; C. Corbel, F. Pierre, P. Hautojärvi, K. Saarinen and P. Moser, Phys. Rev. B 41 (1990) 10632; C. Corbel, F. Pierre, K. Saarinen, P. Hautojärvi and P. Moser, Phys. Rev. B 45 (1992) 3386.
[17] M. Alatalo, H. Kauppinen, K. Saarinen, M.J. Puska, J. Mäkinen, P. Hautojärvi and R.M. Nieminen, Phys. Rev. B 51 (1995) 4176.
[18] M. Alatalo, B. Barbiellini, M. Hakala, H. Kauppinen, T. Korhonen, M.J. Puska, K. Saarinen, P. Hautojärvi and R.M. Nieminen, Phys. Rev. B, in print.
[19] B. Barbiellini, M.J. Puska, T. Torsti and R.M. Nieminen, Phys. Rev. B 51 (1995) 7341.
[20] H.E. Schaefer, W. Stuck, F. Banhart and W. Bauer, in: Proc. 8th Int. Conf. on Vacancies and Interstitials in Metals and Alloys, Eds. C. Ambromeit and H. Wollenberger (Trans Tech, Aedermannsdorf, Switzerland, 1986).
[21] R.H. Howell, Phys. Rev. B 24 (1981) 1835.
[22] D. Herlac, H. Stoll, W. Trost, T.E. Jackman, K. Maier, H.E. Schaefer and A. Seeger, Appl. Phys. 12 (1977) 59.
[23] H.E. Schaefer, R. Gugelmeier, M. Schmolz and A. Seeger, in: Proc. 5th Risø Int. Symp. on Metallurgy and Materials Science, Eds. N.H. Andersen, M. Eldrup, N. Hansen, D.J. Jensen, T. Leffers, H. Lillholt, O.B. Pedersen and B.N. Singh (Risø National Laboratory, Risø, Denmark, 1984).
[24] A. Vehanen, P. Hautojärvi, J. Johansson and J. Yli-Kauppila, Phys. Rev. B 25 (1982) 762.
[25] P. Hautojärvi, H. Huomo, M. Puska and A. Vehanen, Phys. Rev. B 32 (1985) 4326.